PCCP

ROYAL SOCIETY OF CHEMISTRY

PAPER

View Article Online
View Journal | View Issue

Cite this: *Phys. Chem. Chem. Phys.*, 2024, **26**, 9931

Modulation of luminescence properties of circularly polarized thermally activated delayed fluorescence molecules with axial chirality by donor engineering†

Shulei Liu, Songsong Liu, Yang Gao, Lili Lin, Chuan-Kui Wang, Jianzhong Fan * and Yuzhi Song *

Multifunctional thermally activated delayed fluorescence (TADF) materials are currently a trending research subject for luminescence layer materials of organic light-emitting diodes (OLEDs). Among these, circularly polarized thermally activated delayed fluorescence (CP-TADF) materials have the advantage of being able to directly achieve highly efficient circularly polarized luminescence (CPL). The simultaneous integration of outstanding luminescence efficiency and excellent luminescence asymmetry factor (g_{lum}) is a major constraint for the development of CP-TADF materials. Therefore, on the basis of first-principles calculations in conjunction with the thermal vibration correlation function (TVCF) method, we study CP-TADF molecules with different donors to explore the feasibility of using the donor substitution strategy for optimizing the CPL and TADF properties. The results indicate that molecules with the phenothiazine (PTZ) unit as the donor possess small energy difference, a great spin–orbit coupling constant and a rapid reverse intersystem crossing rate, which endow them with remarkable TADF features. Meanwhile, compared with the reported molecules, the three designed molecules exhibit better CPL properties with higher g_{lum} values. Effective molecular design strategies by donor engineering to modulate the CPL and TADF properties are theoretically proposed. Our findings reveal the relationship between molecular structures and luminescence properties of CP-TADF molecules and further provide theoretical design strategies for optimizing the CPL and TADF properties.

Received 25th January 2024,
Accepted 4th March 2024

DOI: 10.1039/d4cp00341a

rsc.li/pccp

1. Introduction

Organic light-emitting diodes (OLEDs) with light weight and bendable properties have been extensively used in optoelectronic lighting and display fields widely.[1–3] As one of the most popular choices for light-emitting layer materials in OLEDs, thermally activated delayed fluorescence (TADF) materials can utilize the reverse intersystem crossing (RISC) process to achieve efficient use of excitons, which is due to the small energy difference between their singlet excited states and the triplet excited states.[4–8] Recently, multifunctional TADF materials have emerged to meet the needs of society. These include multi-stimulus-responsive TADF materials,[9] circularly polarized thermally activated delayed fluorescence (CP-TADF) materials,[10–12] and aggregation-induced TADF materials.[13] Among these, CP-TADF materials show promising development prospects due to their circularly polarized luminescence (CPL), and are widely used in the fields of three-dimensional displays and information encryption.[14,15] Moreover, CPL materials are independent of the polarizing film and 1/4 wave plate, avoiding complex device structures and the loss of luminance intensity.[16] In recent years, more and more attention has been paid to CPL research. In 1997, Meijer *et al.* discovered the circularly polarized electroluminescence (CPEL) effect in chiral polymers.[17] Since then, various CPL materials have been found. However, all of these materials inevitably exhibit efficiency roll-off, which limits the further development of circularly polarized organic light-emitting diodes (CP-OLEDs).

To address this issue, Imagawa *et al.* combined a chiral skeleton with a TADF molecule for the first time, which had a sufficiently small energy difference (ΔE_{ST}) between the first singlet excited state (S_1) and the first triplet excited state (T_1). Moreover, fast RISC could be achieved efficiently, which guaranteed high exciton utilization.[18] They synthesized CP-TADF molecules with central chirality, namely 12-(2-(diphenylamino)-phenyl)-12-hydroxynaphthacen-5(12*H*)-one (DPHN), with which CPL can be achieved with large luminescence asymmetry factor (g_{lum}) and considerable exciton utilization. Recently, Chen *et al.*

Shandong Province Key Laboratory of Medical Physics and Image Processing Technology, School of Physics and Electronics, Shandong Normal University, Jinan 250014, China. E-mail: fanjianzhongvip@163.com, yzsong@sdnu.edu.cn

† Electronic supplementary information (ESI) available. See DOI: https://doi.org/10.1039/d4cp00341a

realized that the large distance between the chiral skeleton and the emitting unit makes the perturbation of the chiral unit small, which limits the enhancement of the CPL properties. Therefore, they designed axially chiral CP-TADF molecules, (−)-(*S*)-Cz-Ax-CN and (+)-(*R*)-Cz-Ax-CN, synthesized by coupling two fluorophores 3-(9*H*-carbazol-9-yl)benzonitrile (Cz-CN). The CP-TADF molecules achieved a g_{lum} of 10^{-2} orders of magnitude and a photoluminescence quantum yield (PLQY) of 68.2%.[19] In 2020, Zheng *et al.* achieved better CPL and TADF properties by replacing one of the carbazole (Cz) units with phenoxazine (PXZ) based on the same chiral skeleton.[20] Therefore, achieving CPL while maintaining high exciton utilization has become a popular research topic in CP-TADF materials.

By changing the donor unit, it is possible to balance the properties of both CPL and TADF. This motivated us to explore the strategy of developing efficient molecules by designing and testing the luminescence properties of CP-TADF molecules with different donor units. The molecular structures in the ground and excited states are optimized using the BMK functional coupled with the 6-31G(d) basis set based on the density functional theory (DFT) and time-dependent density functional theory (TD-DFT) methods, respectively. The photophysical properties including molecular transition properties, intersystem crossing (ISC) and RISC processes, and CPL properties have been investigated in detail theoretically. The effects of donor substitutions on these properties have also been studied. The aim of our study is to propose design strategies for modulating CPL and TADF properties and offer rational suggestion for designing efficient CP-TADF molecules.

2. Theoretical methods and computational details

First, we construct all structures of molecules and use the polarizable continuum method by the Integral Equation Formalism model (IEFPCM) to simulate the liquid phase environment in toluene.[21,22] In order to make our theoretical calculations more reliable, we use different functionals (B3LYP, BMK, M062X, PBE0, and WB97XD)[23–25] combined with the 6-31G(d) basis set[26] for the optimization and frequency analysis of the S_1 state of Cz-Ax-CN in toluene. Fluorescence emission wavelengths are obtained and the corresponding results are listed in Table 1. It is found that the computational data (449 nm) by BMK can well match the experiment result (458 nm). In the DFT and TD-DFT calculations, some approximate methods are adopted to simplify the calculations, such as the case of two-electron integrals and Tamm–Dancoff approximation. Thus, some acceptable differences between theoretical calculations and experimental measurements are generated, such as the difference between 449 nm (computational data) and 458 nm (experiment result). This makes us to think that using the 6-31G(d) basis set to calculate the emission wavelength and other photophysical properties of molecules is reliable, and this method has been recognized in related research studies.[27,28] Therefore, for the subsequent discussion, we employ the BMK functional with the 6-31G(d) basis set. We optimize the structure of S_0 based on the structure we constructed. Then, based on the optimized S_0 structure, the S_1 and T_1 states of the four chiral TADF molecules are optimized by using DFT and TD-DFT to obtain the corresponding molecular structures. All the molecular structures are with no imaginary frequency, which determines the stability of the structures, so we can use the obtained structures to analyze the photophysical properties of the molecules. All the calculations are carried out using the Gaussian 16 program suite.[29]

Table 1 The fluorescence emission wavelengths (nm) of Cz-Ax-CN in toluene calculated using different functionals and experimentally measured wavelengths

	B3LYP	BMK	M062X	PBE0	WB97XD	Exp.
Cz-Ax-CN	572	449	408	534	379	458

Decay rates should also be obtained. The main formulas used in this study are summarized below.

The fluorescence radiative rate is obtained using the Einstein spontaneous emission equation:[30]

$$k_r = \frac{f\Delta E_{fi}^2}{1.499} \quad (1)$$

Here, f represents the oscillator strength of S_1, ΔE_{fi} represents the vertical emission energy (cm^{-1}) between the S_1 and the ground states (S_0) and k_r is defined as the radiative decay rate (s^{-1}).[31]

For the non-radiative process between S_1 and S_0, the non-radiative decay rate (k_{nr}) is obtained from the Fermi's golden rule and Condon approximation:

$$k_{nr} = \frac{2\pi}{\hbar^2}\sum_{u,v} P_{iv}\left|\hat{H}_{fu,iv}\right|^2 \delta(E_{iv} - E_{fu}) \quad (2)$$

Here, P_{iv} represents the Boltzmann distribution function of the initial state and $\hat{H}_{fu,iv}$ represents the interaction between two Born–Oppenheimer states. The $\hat{H}$ can be expressed as:

$$\hat{H}\Psi_{iv} = \hat{H}^{BO}\Phi_i(r, Q)\Theta_{iv}(Q) + \hat{H}^{SO}\Phi_i(r, Q)\Theta_{iv}(Q) \quad (3)$$

$\hat{H}^{BO}$ represents the non-adiabatic coupling. $\hat{H}^{SO}$ represents the spin–orbit coupling (SOC) obtained by the quadratic response function method in the Dalton program.[32,33] r and Q stand for the normal coordinates of electrons and nuclei, respectively. Φ and Θ stand for the electron wave function and nuclear vibration wave function, respectively. Then, according to the Fourier transform of the delta function, we calculate k_{nr} from S1 to S0 as:

$$k_{nr} = \sum_{kl}\frac{1}{\hbar^2}R_{kl}\int_{-\infty}^{\infty} dt\left[e^{i\omega_{if}t}Z_i^{-1}\rho_{ic,kl}(t, T)\right] \quad (4)$$

Here, $\rho_{IC}(t, T) = \mathrm{Tr}\left(\hat{P}_{fk}e^{-i\tau_f\hat{H}_f}\hat{P}_{fl}e^{-i\tau_i\hat{H}_i}\right)$ represents the thermal vibration correlation function (TVCF) in the non-radiative process. All calculation methods and application of these formulas are also used in Shuai, Peng, Cui and our previous works.[34–43] The MOMAP program is used to perform these calculations.[44] The calculations of the SOC constant and

frequency analyses are performed based on the optimized molecular structures of T_1.

Then, in order to characterize the geometric structures of different states, we calculate the root mean squared displacement (RMSD). The calculation formula is as follows:

$$\mathrm{RMSD} = \sqrt{\frac{1}{N}\sum_{i}^{n\mathrm{atom}}\left[(x_i - x_i')^2 + (y_i - y_i')^2 + (z_i - z_i')^2\right]} \quad (5)$$

Here i is the atomic number, and x_i and x_i' are the x-coordinates of the ith atom in the first and the second structures, respectively. y and z have a similar meaning to x. Through this analysis, we can preliminarily predict and compare the photophysical properties of molecules such as the k_{nr}.

Furthermore, to quantitatively characterize the CPL properties, the g_{lum} values can be calculated with the equation:

$$g_{lum} = \frac{4|\mu||m|\cos\theta}{|\mu|^2 + |m|^2} = 4\cos\theta\frac{|m|}{|\mu|} \quad (6)$$

Here, μ and m are the electronic transition dipole moment and magnetic transition dipole moment, respectively, and θ is the angle between them.

Then, the frontier molecular orbital (FMO) analyses and natural transition orbital (NTO) analyses are both achieved using Multiwfn.[45]

3. Results and discussion

Based on the proposed molecule Cz-Ax-CN synthesized by Chen's group,[20] we chose three different donor moieties, 9,10-dihydro-9,9-dimethylacridine (DMAC), PTZ and PXZ, to design new axial chiral TADF molecules named DMAC-Ax-CN, PTZ-Ax-CN and PXZ-Ax-CN by donor substitution engineering, and the corresponding structures are shown in Fig. 1. Then, molecular structures and transition properties as well as radiative and non-radiative decay processes are studied, and the CPL and TADF properties are revealed.

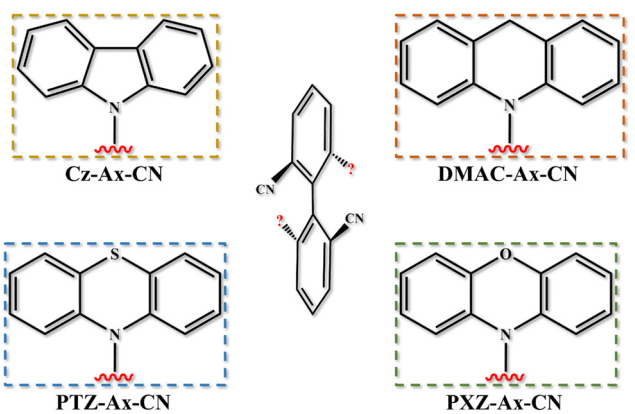

Fig. 1 The structures of the skeleton and donors for all molecules.

3.1. Molecular structures and RMSD values

Identifying the geometry of the CP-TADF molecule is the first step in studying its photophysical properties. Therefore, the structures of the ground and excited states of the four molecules are optimized by applying the BMK functional and the 6-31G(d) basis set and the stability of the structures is ensured by frequency analysis. To compare the structural differences of the molecules in different states, we calculate the RMSD values between the S_0, S_1 and T_1 states of the four molecules. The corresponding results are displayed in Fig. 2. The results show that the RMSD value between S_0 and S_1 is smaller for the Cz-Ax-CN (0.163 Å) and PTZ-Ax-CN (0.193 Å) molecules than the other two molecules (0.853 Å and 0.387 Å). This suggests that these two molecules may have smaller non-radiative quenching rates, which is consistent with our subsequent calculations of k_{nr}. It is found that the RMSD value between S_1 and T_1 is smaller for all molecules. Additionally, the RMSD value of the PTZ-Ax-CN (0.022 Å) molecules is significantly smaller than that of the other three molecules (0.064 Å, 0.086 Å and 0.026 Å), indicating a smaller recombination energy, which may result in a more desirable RISC process.

3.2. Thermally activated delayed fluorescence properties

The performance of TADF materials can be evaluated using the k_{RISC} and k_r values. The variations in the molecular geometry result in differences in the electronic structure, such as energy levels and transition properties, which ultimately affect the TADF process. Thus, we examine these characteristics by investigating the excited state and luminescence properties of the four chiral TADF molecules.

3.2.1. Energy gaps and the frontier molecular orbitals. ΔE_{ST} has a significant impact on the TADF properties of a molecule.[46,47] A small energy difference promotes the RISC process, resulting in a more efficient TADF. To obtain the adiabatic energy of the molecules at S_1 and T_1 states, we optimize the molecular structures to calculate the energy difference. The corresponding data are presented in Table 2. To provide a more intuitive comparison of the energy differences between the four molecules, the ΔE_{ST} diagram is shown in Fig. S1 (ESI†). The results indicate that the energy difference of the three designed molecules (0.06 eV, 0.04 eV and 0.05 eV) is significantly smaller than that of the original molecule (0.12 eV), making it more likely for exciton transitions from T_1 to S_1. Therefore, it is conducive to achieving efficient TADF and luminescence efficiency. To investigate the reason for the change in the energy difference, we calculate the FMOs and the corresponding results are shown in Fig. 3. According to the equation:

$$\Delta E_{ST} = E_S - E_T = 2J \quad (7)$$

$$J = \iint \Phi_L(1)\Phi_H(2)\frac{e^2}{r_1 - r_2}\Phi_L(2)\Phi_H(1)\mathrm{d}r_1\mathrm{d}r_2 \quad (8)$$

where J is the exchange energy of the two unpaired electrons at the excited states, and E_S and E_T are adiabatic energies of S_1 and T_1, respectively. It can be observed that the HOMO of all

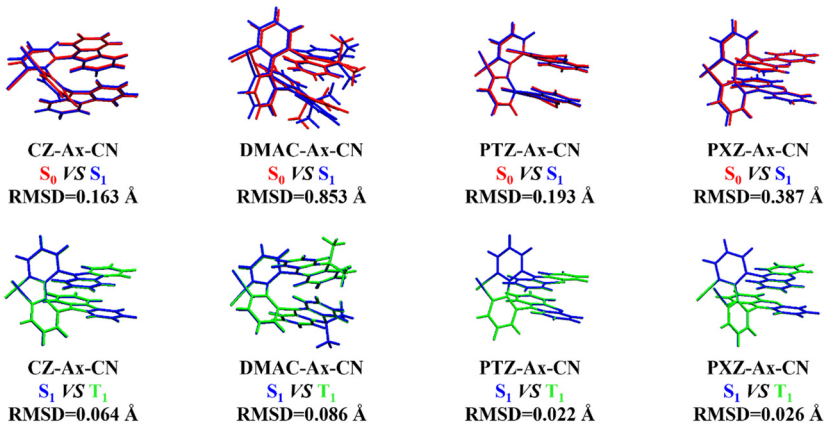

Fig. 2 Geometry comparisons and RMSD values of all molecules between S_0 (red), S_1 (blue), and T_1 (green) in toluene, respectively.

Table 2 Detailed data for Cz-Ax-CN, DMAC-Ax-CN, PTZ-Ax-CN and PXZ-Ax-CN. λ_{em} (nm) is the emission wavelength of the molecule, E_S is the adiabatic energy of the S_1 state, E_T is the adiabatic energy of the T_1 state, ΔE_{ST} is the adiabatic energy difference between the S_1 state and the T_1 state of the molecules, and f is the oscillator strength of the molecules in toluene

	λ_{em} (nm)	E_S (eV)	E_T (eV)	ΔE_{ST} (eV)	f
Cz-Ax-CN	449.20	3.08	2.96	0.12	0.0347
DMAC-Ax-CN	537.27	2.87	2.81	0.06	0.0094
PTZ-Ax-CN	600.68	2.48	2.44	0.04	0.0031
PXZ-Ax-CN	603.16	2.46	2.41	0.05	0.0090

molecules is primarily located on the donor unit, whereas the LUMO is predominantly situated on the acceptor group and chiral skeleton. Moreover, the overlap of molecular frontier orbitals is quantitatively compared using the Multiwfn program, and the corresponding results are listed in Table S1 (ESI†). Therefore, there is more distinct separation of the HOMO and LUMO for the three designed molecules (26.43%, 25.58% and 25.60%) compared to the original molecule (28.31%). This distribution of molecular orbitals is one of the reasons for the decrease in the energy difference for TADF molecules.[48]

To further determine the transition properties of the molecule,[49] we calculate the NTO based on its structures for S_1 and T_1 and the results are presented in Fig. 4, and the enlarged images are shown in Fig. S2 and S3 (ESI†). Chen's group concluded that according to the local-excited (LE) proportion, excited states can be categorized into three types of excitations: the charge-transfer (CT) state (0–40%), the hybrid local-excited and charge-transfer (HLCT) state (40–75%), and the LE state (75–100%).[50–52] According the result, the LE components of the S_1 state for the four molecules are 32.11%, 27.19%, 25.79% and 27.07%, indicating that the S_1 state of all four molecules is the CT state. However, it is worth noting that the T_1 state of all three designed molecules is the CT state and

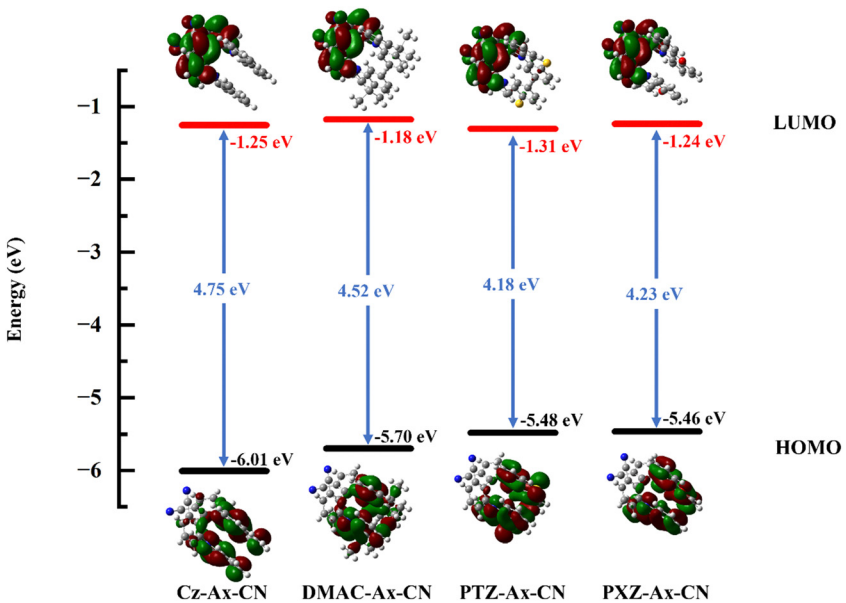

Fig. 3 Energies and distributions of the HOMO and LUMO for all molecules in toluene.

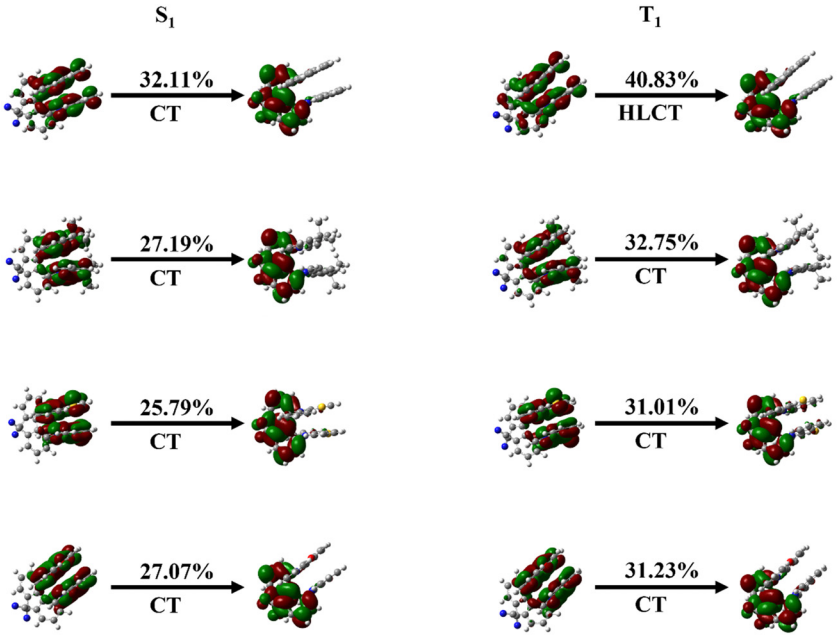

Fig. 4 Natural transition orbitals (NTOs) of the S_1 and T_1 states for Cz-Ax-CN, DMAC-Ax-CN, PTZ-Ax-CN and PXZ-Ax-CN in toluene, respectively.

the T_1 state of the CZ molecule is the HLCT state. According to previous investigation of Penfold,[53–56] when the T_1 state of the molecule is the CT state, such a molecule usually has a smaller ΔE_{ST}. Combining our previous calculations of ΔE_{ST} and current orbital information, our calculations fit well with that conclusion. For the TADF molecule, the electronic properties are more favorable for smaller ΔE_{ST} and facilitate a more desirable RISC process. Moreover, by regulating the geometric structures by donor engineering, which affects the electronic structure and the ΔE_{ST}, it is expected to regulate the TADF properties.

3.2.2. Spin–orbit coupling and decay rates. In addition to the ΔE_{ST}, the TADF properties are also related to the SOC between S_1 and T_1.[57,58] The SOC values of the molecule are calculated and the results are presented in Table 3. Among the four molecules, PTZ-Ax-CN (0.134 cm^{-1}) has a larger SOC value than the other three (0.055 cm^{-1}, 0.066 cm^{-1} and 0.050 cm^{-1}), suggesting a more efficient RISC process. To enhance the intuitive comparison of the conversion processes of the molecules, we calculate the k_{ISC} and k_{RISC} values between S_1 and T_1 using data of SOC and ΔE_{ST}. The corresponding results are listed in Table 4 and are plotted as shown in Fig. S4 (ESI†). It is found that the three designed molecules (3.76×10^6 s^{-1}, 7.67×10^6 s^{-1} and 1.73×10^5 s^{-1}) exhibit a significantly higher k_{RISC} compared to the original molecule (5.62×10^4 s^{-1}). This is closely related to their smaller ΔE_{ST} and larger SOC, which ensures ideal TADF properties. To investigate the energy consumption process, we calculate the k_{nr} of the four molecules. According to the data in Table 4, we discover that the k_{nr} of the three designed molecules (6.82×10^7 s^{-1}, 3.31×10^7 s^{-1} and 5.62×10^7 s^{-1}) is slightly increased compared to that of the Cz-Ax-CN (2.45×10^7 s^{-1}), which is caused by the stronger vibrational coupling effect with smaller energy difference between S_1 and S_0 (shown in Fig. S1, ESI†). In addition, the values of k_r are calculated by combining the oscillator strength (f) obtained from the optimized S_1, and the corresponding data are shown in Table 4. The Cz-Ax-CN has a higher k_r (1.15×10^7 s^{-1}) due to its stronger f (0.0347). Moreover, the DMAC-Ax-CN (0.0094), PTZ-Ax-CN (0.0031), and PXZ-Ax-CN (0.0090) have smaller f, and they also demonstrate considerable k_r (2.17×10^6 s^{-1}, 5.73×10^5 s^{-1} and 1.65×10^6 s^{-1}). Thus, it can be seen that all four molecules have large k_r and efficient emission can be achieved. In summary, based on the donor engineering strategy, three new efficient TADF molecules are proposed.

Table 3 Calculated SOC constants between S_1 and T_1 states for Cz-Ax-CN, DMAC-Ax-CN, PTZ-Ax-CN and PXZ-Ax-CN in toluene based on optimized T_1 structures

Unit: cm^{-1}	$\langle T_1\lvert\hat{H}_{soc}\rvert S_1\rangle$
Cz-Ax-CN	0.055
DMAC-Ax-CN	0.066
PTZ-Ax-CN	0.134
PXZ-Ax-CN	0.050

Table 4 Rate constants of radiative and non-radiative processes from S_1 to S_0 states as well as the ISC and RISC rates between S_1 and T_1 states for all studied molecules in toluene

	k_{ISC} (s^{-1})	k_{RISC} (s^{-1})	k_r (s^{-1})	k_{nr} (s^{-1})
Cz-Ax-CN	4.94×10^5	5.62×10^4	1.15×10^7	2.45×10^7
DMAC-Ax-CN	6.47×10^6	3.76×10^6	2.17×10^6	6.82×10^7
PTZ-Ax-CN	1.90×10^7	7.67×10^6	5.73×10^5	3.31×10^7
PXZ-Ax-CN	1.17×10^6	1.73×10^5	1.65×10^6	5.62×10^7

3.3. Circularly polarized luminescence properties

In order to evaluate the CPL properties of the molecules, the electron circular dichroism spectra (ECD) are calculated using

the Multiwfn program based on the optimized ground state and the corresponding results are shown in Fig. 5.[59,60] The plotted lines in all molecules are symmetric about the *X*-axis, indicating the presence of the cotton effect and verifying the success of the chiral perturbation strategy. This suggests that the molecules are chiral and can achieve circularly polarized luminescence. To compare the CPL properties of the four molecules, we also conduct vertical emission calculations based on the S_1 structure. Combining the result of vertical excitation and vertical emission, we calculate the circularly polarized absorption asymmetry factor (g_{abs}) and the circularly polarized luminescence asymmetry factor (g_{lum}), respectively, and the data are listed in Table S2 (ESI†) and Table 5. Based on these data, it can be observed that the angles between the electronic transition dipole moment (μ) and magnetic transition dipole moment (m) of the four molecules are approximately 180°, with cosine values of −1. This indicates that the two dipole moments are oriented in opposite directions. Research has shown that the CPL properties of chiral molecules can be measured using the g_{lum}. The larger the absolute value of this factor, the better the circularly polarized properties of the molecule. Combined with the theoretical formulas, it is evident that the value of the g_{lum} is primarily influenced by three factors: the μ, m and θ. Our previous study has indicated that the angle between the two dipole moments has the greatest impact on the luminescence asymmetry factor,[61] and we aim to obtain a dipole moment angle with a larger cosine value. From this perspective, for these four axially chiral molecules with some symmetry, their dipole moment angles are almost always optimal, demonstrating the advantage of this design strategy. Simplifying the

Table 5 The data of luminescence asymmetry factor (g_{lum}) for Cz-Ax-CN, DMAC-Ax-CN, PTZ-Ax-CN and PXZ-Ax-CN in toluene

	$\lvert\mu\rvert$ ($\times10^{-18}$ esu cm)	$\lvert m\rvert$ ($\times10^{-20}$ erg G^{-1})	$\cos\theta$	g_{lum} ($\times10^{-2}$)
Cz-Ax-CN	1.806	0.471	−1	−1.04
DMAC-Ax-CN	1.028	0.379	−1	−1.47
PTZ-Ax-CN	0.623	0.348	−1	−2.23
PXZ-Ax-CN	1.058	0.382	−1	−1.45

calculation formula, we can get $g_{lum} = 4\cos\theta\frac{|m|}{|\mu|}$, *i.e.*, the g_{lum} is proportional to the absolute value of the μ and inversely proportional to the absolute value of the m. As the μ is two orders of magnitude larger than that of the m, decreasing the former may be an effective strategy for obtaining better circular polarization properties. To verify this, we plotted a line graph of the g_{lum} and the μ, as shown in Fig. 6. This is consistent with our conjecture and confirms the effect of μ on the nature of CPL. We find that the three designed molecules have a more desirable g_{lum} than the original molecules due to their smaller μ. PTZ-Ax-CN has the smallest μ and the largest g_{lum}. Thus, using the donor engineering strategy, the CPL properties are modulated. Compared with the reported molecule (Cz-Ax-CN), three new efficient CP-TADF molecules (DMAC-Ax-CN, PTZ-Ax-CN and PXZ-Ax-CN) with large RISC rates and large g_{lum} values are theoretically proposed.

4. Conclusion

In summary, through first-principles calculations with the TVCF method, this work validates the design strategy for

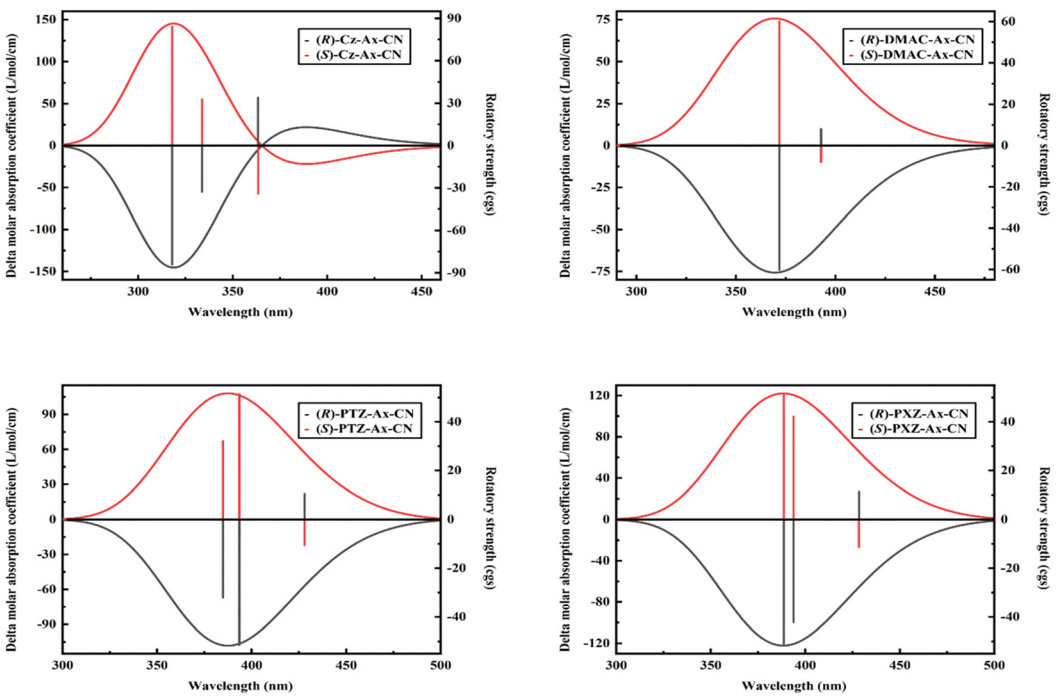

Fig. 5 ECD spectra of Cz-Ax-CN, DMAC-Ax-CN, PTZ-Ax-CN and PXZ-Ax-CN in toluene. The rotatory strength is also illustrated.

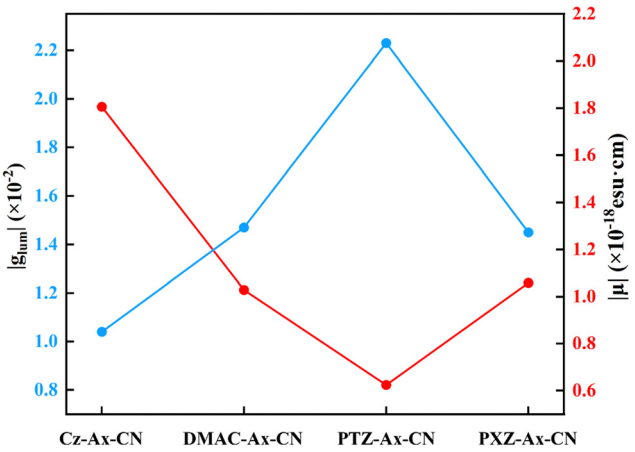

Fig. 6 Calculated luminescence asymmetry factor (g_{lum}) and transition electric dipole moments (μ) of the molecules.

efficient CP-TADF molecules by donor engineering. The results show that modulation of the donor unit can achieve a smaller ΔE_{ST} and a smaller μ for the axial chiral TADF molecule. The former facilitates the RISC process and thus promotes the efficient utilization of the triple excitons, which is essential for effective TADF emission. The latter ensures the desired g_{lum}, which indicates that the molecule can achieve better CPL properties. For three designed molecules, we also observed that the S_1 and T_1 all possess CT features, and this results in smaller ΔE_{ST} required for an efficient RISC process. Additionally, we have computationally verified the relationship between the μ and the g_{lum}. Therefore, it is possible to modulate the μ by regulating the donor unit of CP-TADF materials to achieve a large g_{lum}. Thus, three new efficient molecules with dominant CPL and TADF properties are theoretically proposed, and wise molecular design strategies by donor engineering to modulate the CPL and TADF properties are illustrated. This work reveals the inner relationship between molecular structures and luminescence properties, and could provide theoretical guidance for designing new efficient CP-TADF molecules.

Author contributions

S. L.: writing-original draft; S. L.: visualization; Y. G.: methodology; L. L.: conceptualization and formal analysis; C.-K. W.: supervision; J. F.: writing-review & editing; Y. S.: writing-review & editing.

Conflicts of interest

There are no conflicts of interest to declare.

Acknowledgements

This work was supported by the National Natural Science Foundation of China (Grant no. 11874241, 12274266, 11874242, 21933002 and 12374269). Thanks to Professor Yingli Niu for his great help in the usage of MOMAP.

References

1 T. M. Figueira-Duarte and K. Mullen, Pyrene-Based Materials for Organic Electronics, *Chem. Rev.*, 2011, **111**, 7260–7314.
2 M. A. McCarthy, B. Liu, E. P. Donoghue, I. Kravchenko, D. Y. Kim, F. So and A. G. Rinzler, Low-Voltage, Low-Power, Organic Light-Emitting Transistors for Active Matrix Displays, *Science*, 2011, **332**, 570–573.
3 L. J. Rothberg and A. J. Lovinger, Status of and Prospects for Organic Electroluminescence, *J. Mater. Res.*, 1996, **11**, 3174–3187.
4 C. W. Tang and S. A. VanSlyke, Organic Electroluminescent Diodes, *Appl. Phys. Lett.*, 1987, **51**, 913–915.
5 H. Uoyama, K. Goushi, K. Shizu, H. Nomura and C. Adachi, Highly Efficient Organic Light-Emitting Diodes from Delayed Fluorescence, *Nature*, 2012, **492**, 234–238.
6 S. Hirata, Y. Sakai, K. Masui, H. Tanaka, S. Y. Lee, H. Nomura, N. Nakamura, M. Yasumatsu, H. Nakanotani, Q. Zhang, K. Shizu, H. Miyazaki and C. Adachi, Highly Efficient Blue Electroluminescence Based on Thermally Activated Delayed Fluorescence, *Nat. Mater.*, 2015, **14**, 330–336.
7 D. D. Zhang, X. Z. Song, M. H. Cai, H. Kaji and L. Duan, Versatile Indolocarbazole-Isomer Derivatives as Highly Emissive Emitters and Ideal Hosts for Thermally Activated Delayed Fluorescent OLEDs with Alleviated Efficiency Roll-Off, *Adv. Mater.*, 2018, **30**, 1705406.
8 S. Y. Shao and L. X. Wang, Through-Space Charge Transfer Polymers for Solution-Processed Organic Light-Emitting Diodes, *Aggregate*, 2020, **1**, 45–56.
9 M. L. Yang, I. S. Park, Y. Miyashita, K. Tanaka and T. Yasuda, Mechanochromic Delayed Fluorescence Switching in Propeller-Shaped Carbazole-Isophthalonitrile Luminogens with Stimuli-Responsive Intramolecular Charge-Transfer Excited States, *Angew. Chem., Int. Ed.*, 2020, **59**, 13955–13961.
10 P. Xue, X. Wang, W. J. Wang, J. Y. Zhang, Z. J. Wang, J. B. Jin, C. Zheng, P. Li, G. H. Xie and R. F. Chen, Solution-Processable Chiral Boron Complexes for Circularly Polarized Red Thermally Activated Delayed Fluorescent Devices, *ACS Appl. Mater. Interfaces*, 2021, **13**, 47826–47834.
11 Y. C. Xu, Q. Y. Wang, X. X. Song, Y. Wang and C. L. Li, New Fields, New Opportunities and New Challenges: Circularly Polarized Multiple Resonance Thermally Activated Delayed Fluorescence Materials, *Chem. – Eur. J.*, 2022, **29**, e202203414.
12 G. J. Li, F. Zhan, W. W. Lou, D. Wang, C. Deng, L. N. Cao, Y. N. Yang, Q. S. Zhang and Y. B. She, Efficient Deep-Blue Organic Light-Emitting Diodes Employing Difluoroboron-Enabled Thermally Activated Delayed Fluorescence Emitters, *J. Mater. Chem. C*, 2020, **8**, 17464–17473.

13 Y. Fu, Z. C. Ye, J. P. Xiao, L. Y. Liao, L. F. Chen, Y. X. Mu, S. M. Ji, Z. J. Zhao, H. L. Zhang and Y. P. Huo, Large Effects of Tiny Structural Changes on the AIE-TADF Type Xanthone Derivatives in Mechano-Responsive Luminescence and Electroluminescence, *Dyes Pigm.*, 2022, **205**, 110550.
14 Y. J. Kim, B. Y. Ahn, K. B. Kim and Y. G. Kim, Potential Application of Spintronic Light-Emitting Diode to Binocular Vision for Three-Dimensional Display Technology, *J. Korean Phys. Soc.*, 2006, **49**, 505–508.
15 Y. T. Sang, J. L. Han, T. H. Zhao, P. F. Duan and M. H. Liu, Circularly Polarized Luminescence in Nanoassemblies: Generation, Amplification, and Application, *Adv. Mater.*, 2020, **32**, 1900110.
16 D. W. Zhang, M. Li and C. F. Chen, Recent Advances in Circularly Polarized Electroluminescence Based on Organic Light-Emitting Diodes, *Chem. Soc. Rev.*, 2020, **49**, 1331–1343.
17 E. Peeters, M. P. T. Christiaans, R. A. J. Janssen, H. F. M. Schoo, H. P. J. Dekkers and E. W. Meijer, Circularly Polarized Electroluminescence from a Polymer Light-Emitting Diode, *J. Am. Chem. Soc.*, 1997, **119**, 9909–9910.
18 T. Imagawa, S. Hirata, K. Totani, T. Watanabe and M. Vacha, Thermally Activated Delayed Fluorescence with Circularly Polarized Luminescence Characteristics, *Chem. Commun.*, 2015, **51**, 13268–13271.
19 M. Li, Y. F. Wang, D. D. Zhang, L. Duan and C. F. Chen, Axially Chiral TADF-Active Enantiomers Designed for Efficient Blue Circularly Polarized Electroluminescence, *Angew. Chem., Int. Ed.*, 2020, **59**, 3500–3504.
20 Z. L. Tu, Z. P. Yan, X. Liang, L. Chen, Z. G. Wu, Y. Wang, Y. X. Zheng, J. L. Zuo and Y. Pan, Axially Chiral Biphenyl Compound-Based Thermally Activated Delayed Fluorescent Materials for High-Performance Circularly Polarized Organic Light-Emitting Diodes, *Adv. Sci.*, 2020, **7**, 2000804.
21 J. Z. Fan, S. Qiu, L. L. Lin and C. K. Wang, First-Principles Investigation on Triazine Based Thermally Activated Delayed Fluorescence Emitters, *Chin. J. Chem. Phys.*, 2016, **29**, 291–296.
22 J. Tomasi, B. Mennucci and R. Cammi, Quantum Mechanical Continuum Solvation Models, *Chem. Rev.*, 2005, **105**, 2999–3094.
23 P. J. Stephens, C. F. Chabalowski, F. J. Devlin and K. J. Jalkanen, Ab Initio Calculation of Vibrational Circular Dichroism Spectra Using Large Basis Set MP2 Force Fields, *Chem. Phys. Lett.*, 1994, **225**, 247–257.
24 C. Adamo and V. Barone, Toward Reliable Density Functional Methods without Adjustable Parameters: The PBE0 Model, *J. Chem. Phys.*, 1999, **110**, 6158–6170.
25 A. D. Boese and J. M. Martin, Development of Density Functionals for Thermochemical Kinetics, *J. Chem. Phys.*, 2004, **121**, 3405–3416.
26 S. Hirata and M. Head-Gordon, Time-Dependent Density Functional Theory within the Tamm-Dancoff Approximation, *Chem. Phys. Lett.*, 1999, **314**, 291–299.
27 S. Y. Lin, Q. Ou and Z. G. Shuai, Computational Selection of Thermally Activated Delayed Fluorescence (TADF) Molecules with Promising Electrically Pumped Lasing Property, *ACS Mater. Lett.*, 2022, **4**, 487–496.
28 S. Y. Lin, Q. Ou, Q. Peng and Z. G. Shuai, Aggregation-Enhanced Thermally Activated Delayed Fluorescence Efficiency for Two-Coordinate Carbene–Metal–Amide Complexes: A QM/MM Study, *J. Phys. Chem. Lett.*, 2021, **12**, 2944–2953.
29 M. J. Frisch, G. W. Trucks, H. B. Schlegel, G. E. Scuseria, M. A. Robb, J. R. Cheeseman, G. Scalmani, V. Barone, G. A. Petersson, H. Nakatsuji, X. Li, M. Caricato, A. V. Marenich, J. Bloino, B. G. Janesko, R. Gomperts, B. Mennucci, H. P. Hratchian, J. V. Ortiz, A. F. Izmaylov, J. L. Sonnenberg, D. Williams-Young, F. Ding, F. Lipparini, F. Egidi, J. Goings, B. Peng, A. Petrone, T. Henderson, D. Ranasinghe, V. G. Zakrzewski, J. Gao, N. Rega, G. Zheng, W. Liang, M. Hada, M. Ehara, K. Toyota, R. Fukuda, J. Hasegawa, M. Ishida, T. Nakajima, Y. Honda, O. Kitao, H. Nakai, T. Vreven, K. Throssell, J. A. Montgomery Jr., J. E. Peralta, F. Ogliaro, M. J. Bearpark, J. J. Heyd, E. N. Brothers, K. N. Kudin, V. N. Staroverov, T. A. Keith, R. Kobayashi, J. Normand, K. Raghavachari, A. P. Rendell, J. C. Burant, S. S. Iyengar, J. Tomasi, M. Cossi, J. M. Millam, M. Klene, C. Adamo, R. Cammi, J. W. Ochterski, R. L. Martin, K. Morokuma, O. Farkas, J. B. Foresman and D. J. Fox, *Gaussian 16 Rev. A.03*, 2016.
30 Z. Shuai, Thermal Vibration Correlation Function Formalism for Molecular Excited State Decay Rates, *Chin. J. Chem.*, 2020, **38**, 1223–1232.
31 D. E. Mccumber, Einstein Relations Connecting Broadband Emission and Absorption Spectra, *Phys. Rev.*, 1964, **136**, A954.
32 K. Aidas, C. Angeli, K. L. Bak, V. Bakken, R. Bast, L. Boman, O. Christiansen, R. Cimiraglia, S. Coriani and P. Dahle, The Dalton Quantum Chemistry Program System, *Wiley Interdiscip. Rev.: Comput. Mol. Sci.*, 2014, **4**, 269–284.
33 Dalton. A Molecular Electronic Structure Program. Release Dalton2013, 2014, available from: **https://daltonprogram.org**.
34 Z. G. Shuai and Q. Peng, Excited States Structure and Processes: Understanding Organic Light-Emitting Diodes at the Molecular Level, *Phys. Rep.*, 2014, **537**, 123–156.
35 Y. J. Sun, H. Geng, Q. Peng and Z. G. Shuai, Computational Study on the Charge Transport and Optical Spectra of Anthracene Derivatives in Aggregates, *Chem. Phys. Chem.*, 2020, **21**, 952–957.
36 P. A. Yin, Q. Wan, Y. L. Niu, Q. Peng, Z. M. Wang, Y. X. Li, A. J. Qin, Z. G. Shuai and B. Z. Tang, Theoretical and Experimental Investigations on the Aggregation-Enhanced Emission from Dark State: Vibronic Coupling Effect, *Adv. Electron. Mater.*, 2020, **6**, 2000255.
37 Y. J. Gao, W. K. Chen, T. T. Zhang, W. H. Fang and G. L. Cui, Theoretical Studies on Excited-State Properties of Au(III) Emitters with Thermally Activated Delayed Fluorescence, *J. Phys. Chem. C*, 2018, **122**, 27608–27619.
38 J. Y. Chen, X. X. Xiao, S. Li, Y. Duan, G. Wang, Y. Liao, Q. Peng, H. B. Fu, H. Geng and Z. G. Shuai, A Novel Strategy

toward Thermally Activated Delayed Fluorescence from A Locally Excited State, *J. Phys. Chem. Lett.*, 2022, **13**, 2653–2660.

39 M. Z. Li, F. Y. Li, Q. Zhang, K. Zhang, Y. Z. Song, J. Z. Fan, C. K. Wang and L. L. Lin, Theoretical Verification of Intermolecular Hydrogen Bond Induced Thermally Activated Delayed Fluorescence in SOBF-OMe*, *Chinese Phys. B*, 2021, **30**, 123302.

40 L. L. Lv, K. Yuan, C. D. Si, G. F. Zuo and Y. C. Wang, Mechanism Study of TADF and Phosphorescence in Dinuclear Copper (I) Molecular Crystal Using QM/MM Combined with An Optimally Tuned Range-Separated Hybrid Functional, *Org. Electron.*, 2020, **81**, 105667.

41 L. Y. Peng, W. K. Chen, Z. W. Li, Y. J. Gao and G. L. Cui, QM/MM Studies on Thermally Activated Delayed Fluorescence of A Dicopper Complex in the Solid State, *J. Phys. Chem. C*, 2021, **125**, 27372–27380.

42 K. Zhang, J. Z. Fan, C. K. Wang and L. L. Lin, Highly Efficient T-Shaped Deep-Red Thermally Activated Delayed Fluorescence Emitters: Substitution Position Effect, *Phys. Chem. Chem. Phys.*, 2021, **23**, 21883–21892.

43 H. P. Zou, Y. Y. Ma, H. L. Liu, Q. F. Mu, K. Zhang, Y. Z. Song, L. L. Lin, C. K. Wang and J. Z. Fan, A QM/MM Study on Through Space Charge Transfer-Based Thermally Activated Delayed Fluorescence Molecules in the Solid State, *J. Mater. Chem. C*, 2022, **10**, 517–531.

44 Y. L. Niu, W. Q. Li, Q. Peng, H. Geng, Y. P. Yi, L. J. Wang, G. J. Nan, D. Wang and Z. G. Shuai, MOlecular MAterials Property Prediction Package (MOMAP) 1.0: A Software Package for Predicting the Luminescent Properties and Mobility of Organic Functional Materials, *Mol. Phys.*, 2018, **116**, 1078–1090.

45 T. L. Wu, S. Y. Liao, P. Y. Huang, Z. S. Hong, M. P. Huang, C. C. Lin, M. J. Cheng and C. H. Cheng, Exciplex Organic Light-Emitting Diodes with Nearly 20% External Quantum Efficiency: Effect of Intermolecular Steric Hindrance between the Donor and Acceptor Pair, *ACS Appl. Mater. Interfaces*, 2019, **11**, 19294–19300.

46 T. Chen, L. Zheng, J. Yuan, Z. F. An, R. F. Chen, Y. Tao, H. H. Li, X. J. Xie and W. Huang, Understanding the Control of Singlet-Triplet Splitting for Organic Exciton Manipulating: A Combined Theoretical and Experimental Approach, *Sci. Rep.*, 2015, **5**, 1–11.

47 S. P. Huang, Q. S. Zhang, Y. Shiota, T. Nakagawa, K. Kuwabara, K. Yoshizawa and C. Adachi, Computational Prediction for Singlet-and Triplet-Transition Energies of Charge-Transfer Compounds, *J. Chem. Theory Comput.*, 2013, **9**, 3872–3877.

48 P. Samanta, D. Kim, V. Coropceanu and J. Brédas, Up-Conversion Intersystem Crossing Rates in Organic Emitters for Thermally Activated Delayed Fluorescence: Impact of the Nature of Singlet vs Triplet Excited States, *J. Am. Chem. Soc.*, 2017, **139**, 4042–4051.

49 S. Xu, Q. Q. Yang, Y. F. Wan, R. F. Chen, S. Wang, S. Y. Si, B. C. Yang, D. Liu, C. Zheng and W. Huang, Predicting Intersystem Crossing Efficiencies of Organic Molecules for Efficient Thermally Activated Delayed Fluorescence, *J. Mater. Chem. C*, 2019, **7**, 9523–9530.

50 R. F. Chen, Y. T. Tang, Y. F. Wan, T. Chen, C. Zheng, Y. Y. Qi, Y. F. Cheng and W. Huang, Promoting Singlet/triplet Exciton Transformation in Organic Optoelectronic Molecules: Role of Excited State Transition Configuration, *Sci. Rep.*, 2017, **7**, 6225.

51 L. F. Chen, S. T. Zhang, H. Li, R. F. Chen, L. Jin, K. Yuan, H. H. Li, P. Lu, B. Yang and W. Huang, Breaking the Efficiency Limit of Fluorescent OLEDs by Hybridized Local and Charge-Transfer Host Materials, *J. Phys. Chem. Lett.*, 2018, **9**, 5240–5245.

52 T. T. Liu, X. J. Chen, J. Zhao, W. C. Wei, Z. Mao, W. Wu, S. B. Jiao, Y. Liu, Z. Y. Yang and Z. G. Chi, Hybridized Local and Charge-Transfer Excited State Fluorophores Enabling Organic Light-Emitting Diodes with Record High Efficiencies Close to 20%, *Chem. Sci.*, 2021, **12**, 5171–5176.

53 M. K. Etherington, J. Gibson, H. F. Higginbotham, T. J. Penfold and A. P. Monkman, Revealing the Spin-Vibronic Coupling Mechanism of Thermally Activated Delayed Fluorescence, *Nat. Commun.*, 2016, **7**, 1–7.

54 J. Gibson, A. P. Monkman and T. J. Penfold, The Importance of Vibronic Coupling for Efficient Reverse Intersystem Crossing in Thermally Activated Delayed Fluorescence Molecules, *ChemPhysChem*, 2016, **17**, 2956–2961.

55 Y. Y. Ma, K. Zhang, Y. C. Zhang, Y. Z. Song, L. L. Lin, C. K. Wang and J. Z. Fan, Effects of Secondary Acceptors on Excited-State Properties of Sky-Blue Thermally Activated Delayed Fluorescence Molecules: Luminescence Mechanism and Molecular Design, *J. Phys. Chem. A*, 2020, **125**, 175–186.

56 R. S. Nobuyasu, J. S. Ward, J. Gibson, B. A. Laidlaw, Z. Ren, P. Data, A. S. Batsanov, T. J. Penfold, M. R. Bryce and F. B. Dias, The Influence of Molecular Geometry on the Efficiency of Thermally Activated Delayed Fluorescence, *J. Mater. Chem. C*, 2019, **7**, 6672–6684.

57 J. Gibson and T. Penfold, Nonadiabatic Coupling Reduces the Activation Energy in Thermally Activated Delayed Fluorescence, *Phys. Chem. Chem. Phys.*, 2017, **19**, 8428–8434.

58 M. Y. Wong and E. Zysman-Colman, Purely Organic Thermally Activated Delayed Fluorescence Materials for Organic Light-Emitting Diodes, *Adv. Mater.*, 2017, **29**, 1605444.

59 T. Lu and F. Chen, Calculation of Molecular Orbital Composition, *Acta Chim. Sin.*, 2011, **69**, 2393–2406.

60 K. Shizu, H. Noda, H. Tanaka, M. Taneda, M. Uejima, T. Sato, K. Tanaka, H. Kaji and C. Adachi, Highly Efficient Blue Electroluminescence Using Delayed-Fluorescence Emitters with Large Overlap Density between Luminescent and Ground States, *J. Phys. Chem. C*, 2015, **119**, 26283–26289.

61 S. L. Liu, S. S. Liu, Y. Gao, H. Lan, L. L. Lin, C. K. Wang, J. Z. Fan and Y. Z. Song, Acceptor engineering for modulating circularly polarized luminescence and thermally activated delayed fluorescence properties, *Mater. Today Chem.*, 2023, **33**, 101700.